Application of Improved MCKD Method Based on QGA in Planetary Gear Compound Fault Diagnosis

Xuan Lyu, Zhanqi Hu, Haili Zhou, Qiang Wang

PII: S0263-2241(19)30189-7
DOI: https://doi.org/10.1016/j.measurement.2019.02.071
Reference: MEASUR 6415

To appear in: *Measurement*

Received Date: 14 November 2018
Revised Date: 23 February 2019
Accepted Date: 25 February 2019

Please cite this article as: X. Lyu, Z. Hu, H. Zhou, Q. Wang, Application of Improved MCKD Method Based on QGA in Planetary Gear Compound Fault Diagnosis, *Measurement* (2019), doi: https://doi.org/10.1016/j.measurement.2019.02.071

Application of Improved MCKD Method Based on QGA in Planetary Gear Compound Fault Diagnosis

Xuan Lyu[a,b], Zhanqi Hu[a,b,*], Haili Zhou[a,b], Qiang Wang[a,b]

[a] School of Mechanical Engineering, YanShan University, Qinhuangdao 066004, PR China

[b] Aviation Key Laboratory of Science and Technology on Generic Technology of Aviation Self-Lubricating Spherical Plain Bearing, YanShan University, Qinhuangdao 066004, PR China

Abstract: An improved maximum correlated kurtosis deconvolution (MCKD) method based on quantum genetic algorithm (QGA) named QGA-MCKD is proposed, which can be used for gear and bearing compound fault diagnosis. Two key parameters, filter length (L) and deconvolution period (T) of MCKD, corresponding to each single fault are adaptively selected by QGA. MCKD is set by the obtained key parameters to process the compound fault signal, and each single fault feature related to the single failed part can be extracted. QGA-MCKD was applied to process the simulated and experimental compound fault signals of planetary gear tooth breakage and bearing rolling element damage, and the gear and bearing fault signals were extracted, respectively. Then power spectrum analysis of gear fault signal and envelop spectrum analysis of bearing fault signal were carried out to diagnose the compound faults. The superiority of QGA-MCKD was verified in comparison with direct spectrum analysis and ensemble empirical mode decomposition (EEMD). The stability of QGA-MCKD was verified in the compound fault diagnosis of gear tooth wear and bearing outer race fault. Results show that QGA-MCKD has a good effectiveness in improving the accuracy of gearbox gear and bearing compound fault diagnosis.

Keywords: compound fault diagnosis, maximum correlation kurtosis deconvolution, quantum genetic algorithm, planetary gear, bearing

* Corresponding author
E-mail address: ronghu118@163.com (Z. Hu).

1. Introduction

Planetary gear transmission is widely used in drivetrain of mechanical equipment such as automobile transmission, wind turbine and machine tools due to its advantages of small size, light weight and large transmission ratio. A schematic diagram of planetary gearbox with a fixed ring gear is shown in Fig. 1, which consists of three or more planet gears (P1, P2, P3 …). The planet gears are mounted on the carrier. When the sun gear is the driving gear, the planet gears rotate in the opposite direction to the sun gear by meshing with it, and at the same time drive the carrier to

rotate in the same direction as the sun gear by meshing with the ring gear. Here, ω_s, ω_p, ω_c stand for the rotating speed of sun gear, planet gear and carrier, respectively.

Nomenclature

T	deconvolution period	T_s	period of interest
L	filter length	C	attenuation coefficient
$k(t)$	simulated signal of planetary gear fault signal	f_n	resonant frequency
f_z	meshing frequency of the planetary gear	τ_m	minor fluctuation
f_{r1}	rotation frequency of gear	$u(t)$	unit step function
l	harmonic number of meshing frequency	A_m	modulation signal
A_l	the l-th harmonic amplitude of meshing frequency	A_0	amplitude of A_m
$s(t)$	periodic impact signal simulating the bearing fault	f_{r2}	rotation frequency of the bearing
T_i	time interval of two adjacent impacts	E_p	envelop entropy
$n(t)$	Gaussian white noise	$a(n)$	envelop signal of $x(n)$
$h(t)$	impact signal composed of M single signals	$x(n)$	zero mean signal
p_n	normalization form of $a(n)$	f_s	sampling rate

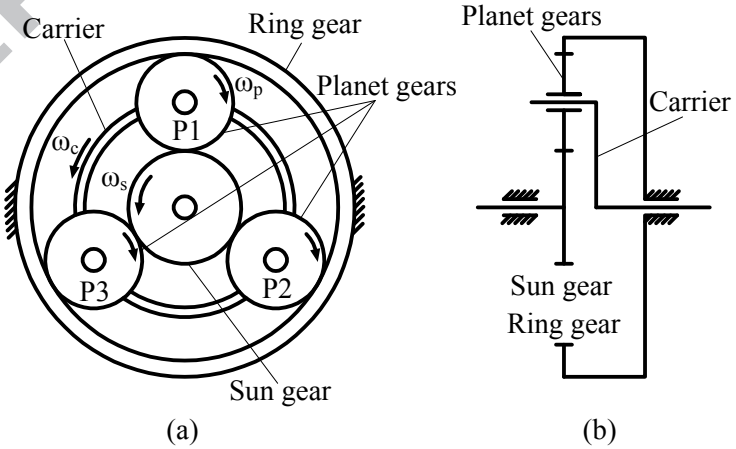

Fig. 1 (a) motion schematic of planetary gear set with the fixed ring gear (b) structure schematic of planetary gear set with the fixed ring gear

However, planetary gearboxes often operate in bad working conditions, so their core components, gears and bearings, are prone to malfunction. The operating states of gears and bearings determine the performance of the entire transmission system, and even affect the service

life of the system. The faults of gears and bearings may cause significant loss of the overall system. Therefore, many researches focus on fault diagnosis of gearbox, aiming to find reliable and effective fault diagnosis methods so as to detect faults as earlier as possible to prevent accidents from happening. Many methods are available for fault diagnosis and condition monitoring of gears and bearings.

Vibration-based fault diagnosis is one of the most commonly used techniques [1-5]. The vibration signal of the fault equipment contains plenty of fault information, and the vibration signal is easy to collect. However, the installation position of sensors is restricted by the equipment under test, and the complicated transmission path may cause coupling of signals, which affects the quality of the measured signal, and increases the difficulty of signal processing.

Fault diagnosis technology based on current analysis [6-8]. The current signal is easy to obtain compared with the vibration signal [9], and the stator current signal has no additional amplitude modulation (AM) effect [8], so the current signal is easier to process. However, this technology is suitable for fault diagnosis of generators or gearboxes of electrical systems, so the current analysis has a limited scope of application.

Acoustic-based fault diagnosis technology is a non-contact, non-destructive diagnosis technique [10-12]. This diagnosis technology has some advantages such as: the acoustic signal is easy to collect and the cost of the technology is low because the acoustic signal can be collected by microphone. However, the acoustic signal is prone to mixing with reflected signal, overlapping signal and other interfering acoustic signals, which can affect the quality of the acoustic signal.

The fault diagnosis technology based on thermal image [13-15] is also a non-contact, non-destructive diagnostic technique. It has the advantages of high sensitivity and good real-time performance. However, the costs of the thermal detection devices are high, and the object to be detected needs to be preheated to a certain temperature to perform diagnosis.

The characteristics of local fault vibration signals of planetary gears are quite different from those of the fixed-shaft gears, and the frequency characteristics are obviously different from those of distributed fault vibration signals. The vibration transmission path between sensors and meshing point of sun gear-planetary gear fault tooth changes because the relative positions between sensors and meshing points of sun gear- planetary gear and planetary gear- internal ring gear change with the rotation of the planet carrier. This time-varying phenomenon of the vibration transmission path

will have an additional amplitude modulation effect on the impact sequence caused by the local fault of the sun gear or the planetary gear [16].

The key to fault diagnosis of planetary gearboxes is how to effectively identify the characteristic frequency and amplitude change of each fault gear or bearing. Gui [17] established a lumped parameter model for a typical planetary gear system with various types of errors, and the influences of tooth faults on time-varying mesh stiffness and tooth impact force were derived analytically. The numerical analysis method based on sideband of the vibration signal was used to detect and localize the fault characteristic frequency of the planetary gear, the sun gear and the internal ring gear. Chen [18] proposed a fault diagnosis method combining ensemble empirical mode decomposition (EEMD) and adaptive stochastic resonance (ASR) in view of complex and weak fault features of planetary gear system. ASR used particle swarm optimization (PSO) algorithm to optimize the critical parameters of stochastic resonance (SR). The signal reconstructed by EEMD was inputted into ASR system, and the weak fault features of planetary gear were extracted. Li [19] proposed a method of planetary gear fault diagnosis via feature image extraction based on multi central frequencies and vibration signal frequency spectrum. The feature bands were extracted by central frequencies decomposed by variational modal decomposition (VMD) to construct the feature images of fault signals, and identified fault signals by the convolution neural network (CNN). He [20] proposed a new deep-learning-based method for wind turbine planetary gearbox fault diagnosis. A sparse representation of the raw vibration signals was generated by shift-invariant sparse coding based on the learned dictionary accomplished by LAMSTAR network with dictionary learning (LAMSTAR-DL), and an optimized large memory storage and retrieval (LAMSTAR) classifier network was trained and used for planetary gearbox fault diagnosis.

A small incipient fault in gear or bearing may cause compound faults in gear-bearing system [21]. Compared with background noise, the fault signal of gearbox is much weaker, and the fault features are even lost in the background noise. In the vibration signal of compound faults, each single fault signal is coupled to other ones, which makes the frequency characteristics of fault signal complicated and difficult to identify. The study of gearbox compound fault diagnosis has gained abundant achievements, and many methods have been proved to be with high practical value. Some methods have been successfully applied in compound fault diagnosis of gearbox,

such as morphological component analysis(MCA) [22] and its improved method [23], ensemble empirical mode decomposition(EEMD) [24], maximum correlated kurtosis deconvolution(MCKD) [25], resonance based signal sparse decomposition(RSSD) [26], blind source separation(BSS) [27], empirical wavelet transform(EWT) [28], and comprehensive application of various methods [29].

Among compound fault diagnosis methods of gearbox, MCKD can extract weak periodic impulse components of the signal in the case of very low SNR, which is suitable for fault diagnosis in strong background noise. The research of MCKD in fault diagnosis of gearbox can be divided into two types. Type I employs MCKD as signal preprocessing tool, and combines MCKD with other methods as comprehensive diagnosis methods. Jia [30] used MCKD as preprocessing tool to highlight the periodic impulse component of signals in the improvement of spectral kurtosis (SK) method, and then the resonant frequency band of the signal after MCKD filtering was selected by SK. The method was successfully applied to diagnose the early fault of bearing. Hong [31] used MCKD and multi-scale wavelet as signal preprocessing and post-processing technologies, respectively, to enhance the effect of de-noising, and successfully identified the compound fault diagnosis of aero-engine rotor in the study of compound fault diagnosis of rotating machinery. Type II aims to improve the performance of MCKD by researching the adaptive parameters selection. Miao [32] proposed an improved MCKD method IMCKD, which could adaptively select the displacement number M and deconvolution period T. This method was used in bearing fault diagnosis, and the fault features were successfully extracted. Tang [25] proposed an improved MCKD method named adaptive MCKD (AMCKD). By using cuckoo search algorithm (CSA), the length of filter L and displacement number M could be adaptively selected. This method was used in compound fault diagnosis of bearing inner race and outer race, and the two fault features were extracted from mixed signal successfully.

This paper focuses on the application of MCKD in diagnosis of planetary gear and bearing compound faults. According to the advantages of MCKD that it can not only eliminate the influence of signal transmission path, but also suppress the background noise interference [33], MCKD can be applied to the processing of compound fault vibration signal of planetary gearbox. The diagnosis performance of MCKD is determined by two key parameters: deconvolution period T and filter length L. The determination of T requires certain prior knowledge, that is, the period of

interested impulse component needs to be known in advance, and the determination of L is general according to previous research results or experience. This will bring great subjective factors to the parameters selection, which may get improper parameters and negatively affect the diagnosis results.

As indicated by the discussion above, the diagnosis performance of MCKD is directly affected by the key parameters. The key parameters are reasonable or not determines whether single fault signals can be successfully extracted from the mixed signal, thereby determining the effect of compound fault diagnosis of the planetary gearbox. So the reasonable parameter selection method is the key to realize the compound fault diagnosis of MCKD in planetary gearbox. In order to overcome the insufficiency of MCKD in parameter selection and improve the diagnosis quality, a method of adaptive parameter selection named QGA-MCKD is proposed, which utilizes advantages of QGA such as strong global searching ability and the computational accuracy is not limited by population size [34-36], to adaptively search for the best parameter combination. Firstly, QGA is used to select optimal parameters L and T adaptively. Then, the optimal parameters are used to set MCKD and process the raw signal to extract single fault signals. Finally, power spectrum or envelop spectrum analysis is performed to identify the characteristic frequency. This method was used in compound fault diagnosis of planetary gearbox, and satisfactory results were obtained.

The rest of this paper is composed as follows: In Section 2 the principles of MCKD and QGA are introduced. In Section 3 the core principle of the proposed method is expounded. The effectiveness of the proposed method is validated in Sections 4 by simulated signals and experimental signals, respectively. In Section 5 concluding remarks are drawn.

2. Theoretical background

QGA-MCKD comprehensively considers the advantages of QGA in global optimization and calculation efficiency, to solve the problem that the diagnosis results may be inaccurate caused by improper parameters due to the traditional MCKD parameter selection method, thereby maximizing the advantages of MCKD in fault diagnosis.

2.1. Theory of MCKD

MCKD was proposed by McDonald [33] in 2012 and successfully used in the fault diagnosis of gear tooth surface peeling off.

Assume that the fault signal of the rotating machine is

$$y = h * x + e \tag{1}$$

where, y is output signal measured by the sensor, x is the input signal, h is the transfer function of the signal transmitted in the surrounding environment and the propagation medium, and e is the noise signal.

The optimization function of MCKD is expressed as [11]:

$$CK_M(T) = \frac{\sum_{n=1}^{N}\left(\prod_{m=0}^{M} y_{n-mT}\right)^2}{\left(\sum_{n=0}^{N} y_n^2\right)^{M+1}} \tag{2}$$

where, M is the displacement number, and T is the deconvolution period which can be calculated as follows.

$$T = f_s \cdot T_s \tag{3}$$

where, f_s is the sampling rate, and T_s is the period of interest.

The purpose of MCKD is to find an FIR filter f that maximizes the correlation kurtosis of the input signal x, so that the input signal x can be recovered according to the output signal y.

$$x = f * y = \sum_{k=1}^{L} f_k x_{n-k+1} \tag{4}$$

where, $\vec{f} = [f_1\ f_2 \cdots f_L]$ is filter coefficient of length L.

The filter coefficient f_k, which corresponds to the maximum correlated kurtosis, can be obtained by solving the derivatives of the numerator and denominator of $CK_M(T)$

$$\frac{d}{df_k} CK_M(T) = 0, k = 1, 2, \cdots, L \tag{5}$$

$$\vec{f} = \frac{\|\vec{y}\|}{2\|\vec{\beta}\|^2}\left(X_0 X_0^T\right)^{-1} \sum_{m=0}^{M} X_{mT} \vec{\alpha}_m \tag{6}$$

where,

$$X_{mT}=\begin{bmatrix} x_{1-mT} & x_{2-mT} & x_{3-mT} & \cdots & x_{N-mT} \\ 0 & x_{1-mT} & x_{2-mT} & \cdots & x_{N-1-mT} \\ 0 & 0 & x_{1-mT} & \cdots & x_{N-2-mT} \\ \vdots & \vdots & \vdots & \ddots & \vdots \\ 0 & 0 & 0 & \cdots & x_{N-L-mT+1} \end{bmatrix}_{L\times N} \quad \vec{\beta}=\begin{bmatrix} y_1 y_{1-T}\cdots y_{1-MT} \\ y_2 y_{2-T}\cdots y_{2-MT} \\ \vdots \\ y_N y_{N-T}\cdots y_{N-MT} \end{bmatrix}_{N\times 1}$$

$$\vec{\alpha}_m=\begin{bmatrix} y_{1-mT}^{-1}\left(y_1^2 y_{1-T}^{2}\cdots y_{1-mT}^{2}\right) \\ \vdots \\ y_{N-mT}^{-1}\left(y_N^2 y_{N-T}^{2}\cdots y_{N-mT}^{2}\right) \end{bmatrix}_{N\times 1}$$

2.2. Theory of QGA

QGA was proposed by K.H.Han [37] in 2000. Based on some concepts and theories of quantum computing, the algorithm uses qubit coding to represent chromosomes, and uses the operations and updates of quantum gate to complete evolutionary search. It has the following characteristics: (1) the performance of the algorithm is not limited by population size; (2) the convergence speed is fast; (3) it has strong global optimization ability.

A qubit is a two-state quantum system that acts as a physical medium for information storage units. The difference between a qubit and a classical bit is that it can be in the superposition state of two quantum states at the same time, and the state of which is

$$|\varphi\rangle = \alpha|0\rangle\beta|1\rangle \tag{7}$$

where, α and β are complex numbers that specify the probability amplitudes of the corresponding states. Normalization of the state to unity guarantees

$$|\alpha|^2+|\beta|^2 = 1 \tag{8}$$

where, $|0\rangle$ and $|1\rangle$ denote the state of spin down and spin up, respectively. A qubit may be in the '1' state, in the '0' state, or in any superposition of the two.

If there is a system of m-qubits, the system can represent 2^m states at the same time. The chromosome composed of m qubits can be expressed as

$$\begin{bmatrix} \alpha_1 & \alpha_2 & \cdots & \alpha_m \\ \beta_1 & \beta_2 & \cdots & \beta_m \end{bmatrix} \tag{9}$$

In quantum theory, the transition between quantum states is mainly realized by quantum gates. As the executive mechanism of evolutionary operations, quantum gates can be selected according

to specific problems. At present, there are many kinds of quantum gates. According to the calculation characteristics of QGA, quantum rotation gates are selected to realize the mutation update of quantum chromosomes. Since the information of the optimal individual is considered in the rotation of the angle, under the guidance of the optimal individual information, the population can be better oriented to the optimal solution, thereby accelerating the convergence of the algorithm. The update operation of quantum rotation gates is

$$U(\theta_i) = \begin{bmatrix} \cos(\theta_i) & -\sin(\theta_i) \\ \sin(\theta_i) & \cos(\theta_i) \end{bmatrix} \tag{10}$$

The update process is as follows

$$\begin{bmatrix} \alpha_i' \\ \beta_i' \end{bmatrix} = U(\theta_i) \begin{bmatrix} \alpha_i \\ \beta_i \end{bmatrix} = \begin{bmatrix} \cos(\theta_i) & -\sin(\theta_i) \\ \sin(\theta_i) & \cos(\theta_i) \end{bmatrix} \begin{bmatrix} \alpha_i \\ \beta_i \end{bmatrix} \tag{11}$$

where, $(\alpha_i, \beta_i)^T$ and $(\alpha_i', \beta_i')^T$ denote the probability amplitude of the i-th qubit rotation gate before and after updating the chromosome, respectively.

According to equation (11), α_i' and β_i' can be expressed as follows

$$\begin{cases} \alpha_i' = \alpha_i \cos(\theta_i) - \beta_i \sin(\theta_i) \\ \beta_i' = \alpha_i \sin(\theta_i) + \beta_i \cos(\theta_i) \end{cases} \tag{12}$$

θ is the rotation angle, the size and direction of which depends on the rotation angle adjustment strategy. The concrete calculation process of QGA is as follows:

(1) Initialize population $Q(t_0)$: initialize the genes of all chromosomes in the population as $(1/\sqrt{2}\ 1/\sqrt{2})$, which indicates that all states of the chromosomes at the beginning of the search appear with the same probability.

(2) Perform coding and individual measurement for the generating units in the population $Q(t_0)$, and get the corresponding deterministic solution $P(t_0)$.

(3) Perform individual measurement to each object in $P(t_0)$. Use a fitness evaluation function to evaluate each individual object in $P(t_0)$ and keep the best object in the generation.

(4) If a satisfactory solution is obtained, stop the algorithm; otherwise, continue to the fifth step.

(5) Use a proper quantum rotation gate U(t) to update $P(t_0)$, and obtain the new population Q(t+1).

(6) Record the optimal individual and the corresponding fitness;

(7) Add 1 to the number of iterations t and then return to step (4).

3. The improved MCKD method based on QGA

When the rotating equipment runs smoothly at a specific input power, the main frequency parameters of each rotating component (such as the rotation frequency of the shaft, the meshing frequency of the gear, the characteristic frequency of the bearing and the fault frequency of the fault bearing, etc.) can be calculated. However, in actual working conditions, there are some influence factors such as slight input power fluctuations, manufacturing or assembly error and wear or even faults caused by equipment operation, so that the frequency of interest does not exactly match the theoretical value. Therefore, the value of the corresponding deconvolution period T is not fixed, but fluctuates within a certain range centered on the theoretical period. When the measured signal is processed by MCKD using the theoretical value for T, the processing result may be inaccurate.

In MCKD there is interaction effect between two key parameters, L and T, and the influence of which on the deconvolution result cannot be ignored. Therefore, there are two challenges in MCKD parameter selection: (1) How to find the optimal parameter T within a given parameter range. (2) How to find the optimal parameter L while searching for the parameter T, so that the two parameters work together to make MCKD achieve the best calculation effect. Choosing the best combination of parameters is the key to use MCKD for gearbox compound fault diagnosis.

As an effective and robust optimization method, QGA can achieve global optimization in a given search space. QGA is used to automatically search the calculation parameters L and T of MCKD, which can overcome the influence of subjective factors and improve the accuracy of fault diagnosis. Based on this, the QGA-MCKD method is established.

To adaptively select parameters using QGA, it is necessary to determine a fitness function as a basis for judging whether the result is the optimal solution. Each time the population is updated, the value of fitness function is calculated. Within the population, the optimal solution in the population group is selected by comparing the fitness value, and the comparisons of optimal solution between populations are used to determine whether to continue updating the population and the direction of movement of the population. So the optimal results can be obtained.

The envelope entropy (EE) of the deconvolution signal processed by MCKD is used as the fitness function of the optimization method. The EE value of the deconvolution signal is used as the basis for judging the optimization result.

The envelop entropy E_p of zero mean signal $x(n)$ ($n = 1, 2, \cdots N$) can be expressed as follows

$$\begin{cases} E_p = -\sum_{n=1}^{N} p_n \lg p_n \\ p_n = a(n) \Big/ \sum_{n=1}^{N} a(n) \end{cases} \tag{13}$$

where, p_n is the normalization form of $a(n)$, and $a(n)$ is the envelop signal of $x(n)$ demodulated by Hilbert.

If the parameters of MCKD are selected accurately, the deconvolution signal will contain obvious periodic impulse components, and the EE value is small. If the parameters of MCKD are not properly selected, the deconvolution effect is not good, and the periodic impulse components are not obvious, so the envelope entropy value is large. Therefore, the minimum value of the fitness function is used for judging whether the optimal result is obtained.

The flowchart of QGA-MCKD for compound fault diagnosis is illustrated in Fig. 2, and the detailed procedures are as follows:

(1) According to the operating parameters of the gearbox and the fault characteristic period formula of bearings, the characteristic periods of gear (T_{sz}) and that of bearing (T_{si}) are obtained, respectively. The selection ranges of the characteristic period (T_{sz}-T_{sz1}, T_{sz}+T_{sz1}), (T_{si}-T_{si1}, T_{si}+T_{si1}) can be set according to the actual situation, where T_{sz1} and T_{si1} are the maximum fluctuation values allowed for the gear and bearing characteristic periods, respectively. T_{z1}, T_{i1} can be determined according to the monitoring of the rotating speed of the diagnostic object, or according to a reasonable threshold set for the rotating speed fluctuation range of the diagnostic object.

Substituting the selection ranges of the characteristic periods into equation (3) to calculate the corresponding deconvolution periods, respectively, and the selection ranges T of the gear and bearing are obtained.

(2) Initialize the variables of QGA. When initialize the variables of QGA, the relationship between calculation accuracy and computational cost must be considered. A larger population can improve the calculation accuracy, but increase the computational cost. The maximum iteration number needs to be reasonably selected according to the actual working conditions. Excessive iteration number will cause computation redundancy, resulting in waste of time and resources. It is found that the optimal solution can be obtained within 50 generations in this research. Larger filter

lengths can improve the effect of diagnosis [33], but increase the expense of computation. So the population size is set to 30, the maximum number of iterations is set to 50, the selection range of L is set to (2,700), and the parameter T is set according to step 1.

(3) Execute QGA to adaptively search for the optimal parameter combination (L, T). The optimal MCKD parameter combinations (L_z, T_z) and (L_i, T_i) for gear and bearing are obtained, respectively.

(4) Assign the optimal paremeter combinations to MCKD and obtain the output signals.

(5) Perform Hilbert envelope demodulation on the bearing fault signal and power spectrum analysis on the gear fault signal.

(6) Diagnose the fault type of gear and bearing, respectively, according to the extracted characteristic frequency information.

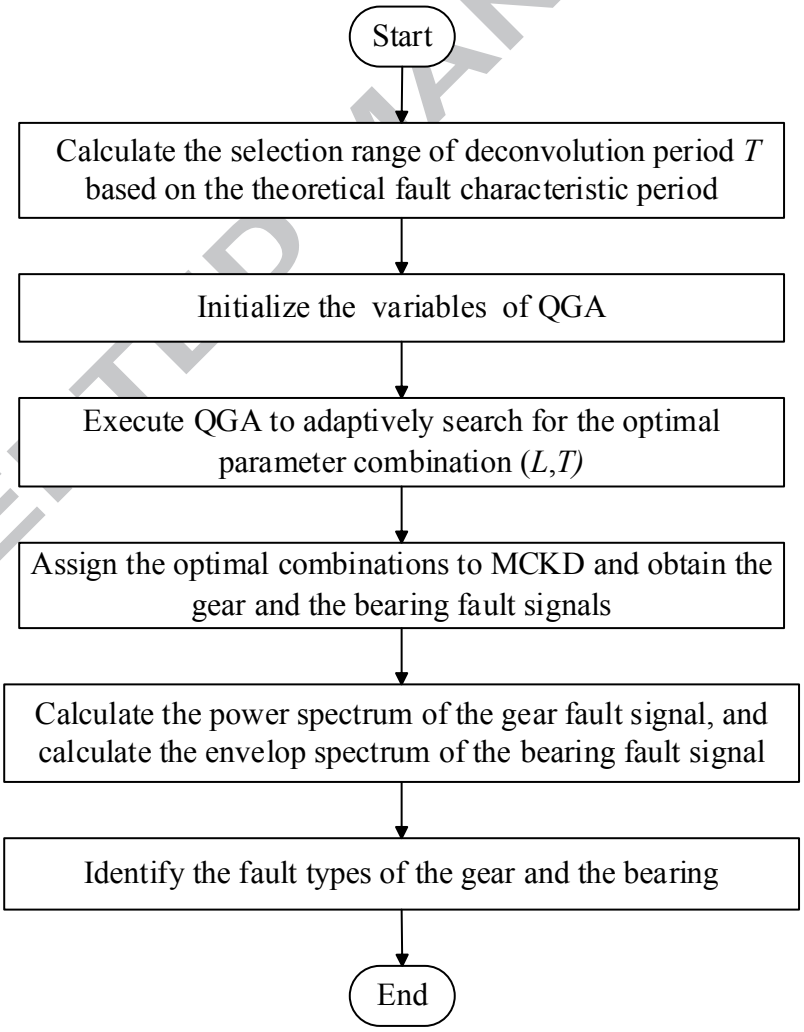

Fig. 2 The flowchart of QGA-MCKD

4. Application of QGA-MCKD

The effectiveness of QGA-MCKD was verified by processing the simulated signal and the

experimental signal. The superiority of the proposed method was verified by comparing the signal processing effect of QGA-MCKD with direct spectrum analysis (power spectrum and envelop spectrum) and EEMD.

The simulated signal is composed of a modulated signal simulating the planetary gear fault and a periodic impact signal simulating the bearing fault, and the experimental signal is collected from a test platform with a one tooth breakage planetary gear and a one rolling element damage bearing.

4.1. Application of QGA-MCKD in the simulated signal

The simulated signal of planetary gearbox compound fault is set as follows, and the simulated signal is used as the deconvolution signal:

$$\begin{cases} x(t) = k(t) + s(t) + n(t) \\ k(t) = \sum_{l=1}^{n} A_l[1+\cos(2\pi f_{r1}t)]\cos(2\pi f_z t) \\ s(t) = \sum_{m=1}^{M} A_m h(t - mT_i - \tau_m) + n(t) \\ h(t) = \exp(-Ct)\sin(2\pi f_n t)u(t) \\ A_m = 1 - A_0\sin(2\pi f_{r2}t) \end{cases} \tag{14}$$

where, $k(t)$ is the modulated signal to simulate the planetary gear fault in which f_z is the carrier frequency to simulate the meshing frequency of planetary gear, f_{r1} is the modulation frequency to simulate the rotation frequency of gear, l is harmonic number of the meshing frequency and A_l is the l-th harmonic amplitude of meshing frequency. $s(t)$ is periodic impact signal simulating the bearing fault and $n(t)$ is Gaussian white noise. $h(t)$ is composed of M single signals whose attenuation coefficient is C and resonant frequency is f_n. Where, T_i is the time interval of two adjacent impacts, the fault frequency is $f_i=1/T_i$, τ_m is a minor fluctuation of the m-th impact relative to the period T obeying normal distribution, whose standard deviation is 0.5% of the rotation frequency. $u(t)$ is unit step function. A_m is the modulated signal with amplitude A_0, and f_{r2} is the rotation frequency of the bearing. The parameter values of the simulated signal are shown in Table 1.

Table 1 Simulated signal parameter values

f_{r1}(Hz)	f_{r2}(Hz)	f_z(Hz)	f_n(Hz)	T_i(s)	l	A_l(m/s^2)	A_0(m/s^2)	C	M	SNR(dB)
20	10	200	800	1/60	3	[0.03,0.02,0.01]	0.3	600	60	-8

The sampling frequency of the simulated signal is 12kS/s, and the number of sampling points is 12000. Substituting each parameter in Table 1 into equation (14), the time-domain and

frequency spectrum of the simulated signal of fault gear, the simulated signal of fault bearing and their mixed signal with noise can be obtained as shown in Fig. 3, respectively. As shown in Fig. 3(a) and (c), periodic components can be seen clearly, but after adding noise signal, periodic components of the mixed signal are completely submerged as shown in Fig. 3(e). It can be seen in Fig. 3(b) that the main component of power spectrum is composed of meshing frequency and its harmonics, and both of which are modulated by the gear rotation frequency. The significant information related to the fault types cannot be recognized in the power spectrum and envelope spectrum of mixed signal shown in Fig. 3(f) and Fig. 4, respectively.

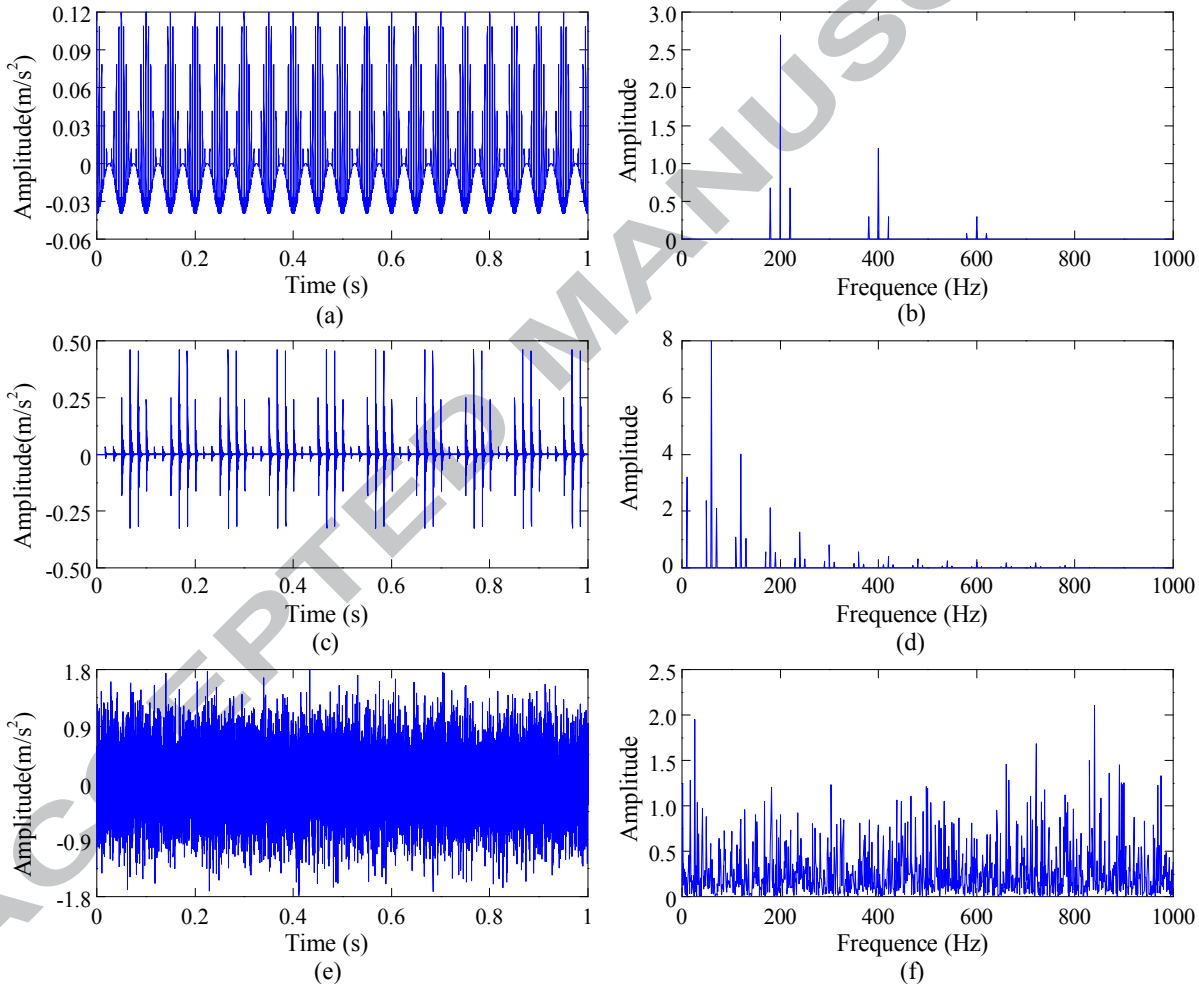

Fig. 3 Time-domain graph and frequency spectrum of the single fault signals and the mixed signal: Time-domain graph and power spectrum of the fault gear modulated signal (a) and (b); time-domain graph and envelop spectrum of bearing impact signal (c) and (d); time-domain graph and power spectrum of the mixed signal (e) and (f).

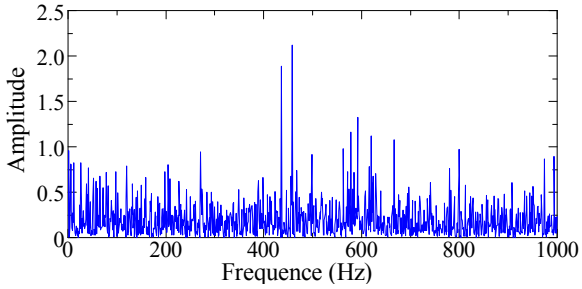

Fig. 4 Envelop spectrum of the mixed signal

QGA was used to optimize the MCKD parameter combination of gear and bearing fault features. The optimization results are shown in Fig. 5(a) and (b).

As show in Fig. 5(a) and (b), with the increasing of iteration number, the EE value of the fault signal obtained by QGA decreases continuously. When the iteration number reaches the 24th generation, the optimal solution of the parameter combination of gear fault signal is stable, and the EE value obtained is 3.91. When the iteration number reaches the 32nd generation, the optimal solution of the parameter combination of bearing fault signal is stable, and the EE value obtained is 4.01. The optimal parameter combination of the gear fault signal is L=270, T=59 and that of the bearing fault signal is L=660, T=198.

Assigned the optimal parameter combinations to MCKD to process the mixed signal, and then the gear and bearing fault signals were obtained, respectively, as shown in Fig. 5(c) and (d). In order to observe the periodic component of the time-domain graph clearly, the gear fault signal is only shown the first 0.1s and the bearing fault signal is only shown the first 1s. As shown in Fig. 5(c) and (d), the periodic components are prominent after the mixed signal being processed.

The power spectrum of the gear fault signal is shown in Fig. 5(e), from which the meshing frequency and its harmonics are the most obvious, and the side frequency component generated by gear rotation frequency modulation also can be seen. Compared with Fig. 3(f), the characteristic frequency of the planetary gear is more obvious, and the fault feature is easier to identify. In the envelope spectrum of bearing fault signal shown in Fig. 5(f), it can be seen that the bearing fault frequency and its harmonics are obvious. Compared with the envelope spectrum of the mixed signal shown in Fig. 4, the main frequency components are much clearer, the harmonic components of the bearing fault frequency are also prominent, and the fault feature of the bearing is easy to recognize.

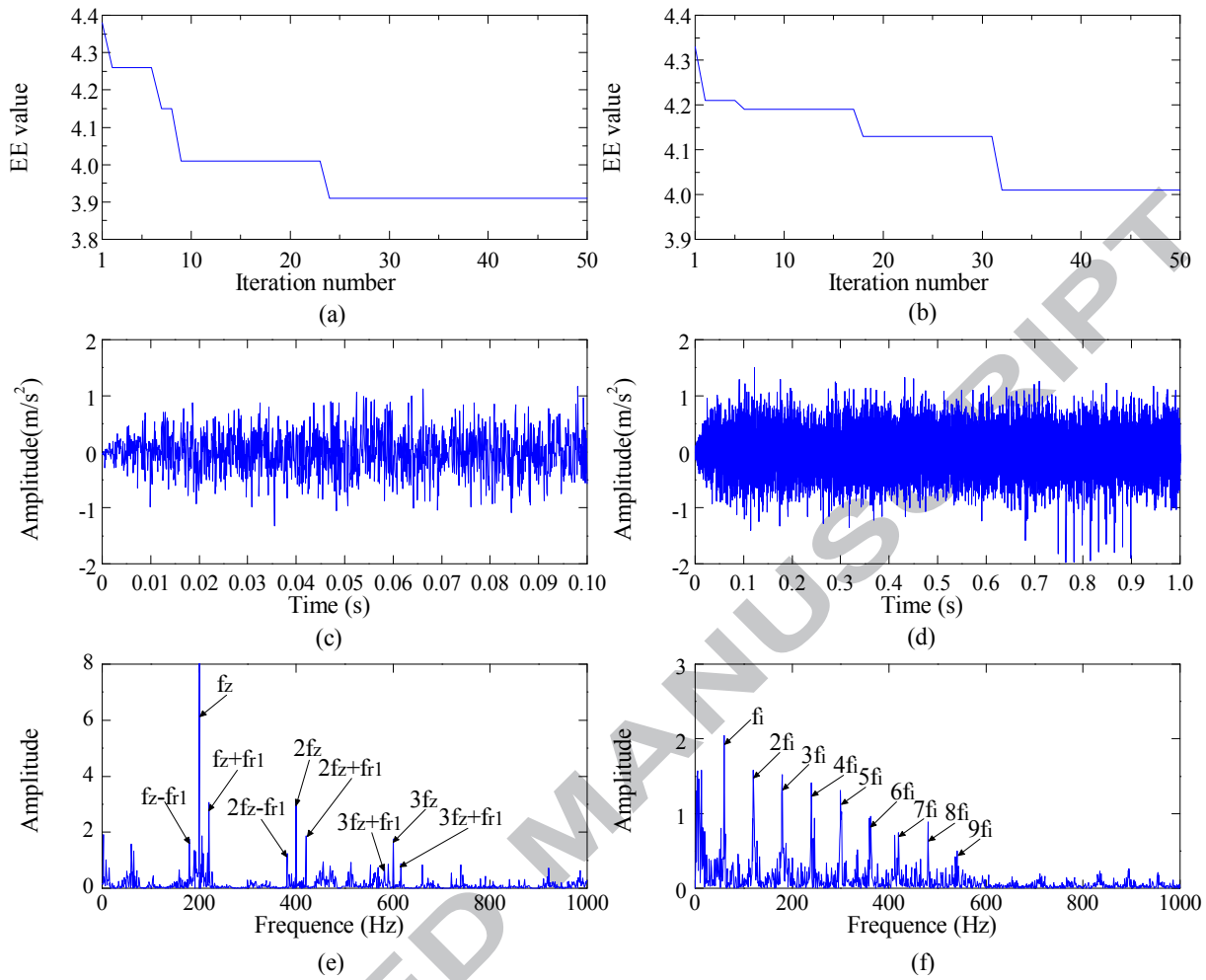

Fig. 5 Results of the mixed signal using QGA-MCKD: (a) and (b) convergence curves of QGA for extracting the gear and bearing fault signals, respectively; (c) and (d) time-domain graphs of the extracted gear and bearing fault signals, respectively; (e) power spectrum of (c); (f) envelope spectrum of (d).

It can be seen from the comparison between QGA-MCKD and direct spectrum analysis that the proposed method can extract fault feature components from the mixed signal contaminated by noise. In order to further verify the superiority of the proposed method, a mature fault diagnosis method EEMD was adopted to compare with QGA-MCKD. The same simulated signals were processed by the two methods, respectively, and the results were compared and verified.

EEMD can decompose a signal into a set of complete and almost orthogonal components named intrinsic mode function (IMF). According to the characteristic of white noise with uniform spectrum distribution, a random Gaussian white noise sequence with uniform scale characteristics and constant amplitude standard deviation coefficient is added to the signal multiple times to smooth the singular points. The effect can avoid pattern confusion caused by signal decomposition [38]. EEMD and EMD are suitable for processing nonlinear and non-stationary signals [39].

The mixed signal was processed using EEMD, and 12 IMFs were acquired, of which the first 5 IMFs contained useful information. As shown in Fig. 6(b), the meshing frequency (f_z) and its

modulation frequency, the second harmonic ($2f_z$) and its modulation frequency, and the third harmonic ($3f_z$) can be seen in IMF 5, IMF 4 and IMF 3, respectively. But because of the noise interference, the amplitude of $2f_z$ is the highest, the amplitude of f_z is smaller than f_z-f_{r1}, and the modulation frequency of $3f_z$ is lost in irrelevant spectral lines. From the envelope spectrum shown in Fig. 6(c), it can be seen that the fault frequency of the bearing and its second and third harmonics appear in IMF3, but there are many irrelevant spectral lines, and the high-order harmonics cannot be recognized. The frequency components related to the gear and bearing faults can be identified using EEMD. However, the fault characteristic frequencies are surrounded by numerous background noise and irrelevant spectral lines, which is prone to misjudging the fault types.

Compared with Fig. 6(c), it can be seen in Fig. 5(f) that the main frequency components of envelop spectrum of the bearing fault signal are more obvious, the interference spectral lines are much less, the high-order harmonic components of the bearing fault frequency are more prominent, and the fault characteristic of the bearing can be recognized more easily. Compared with Fig. 6(b), Fig. 5(e) shows that the characteristic frequencies of the planetary gear are obvious, and the fault feature is easy to identify. These results prove that the proposed method has a better effect in diagnosing the simulated signal than that of EEMD.

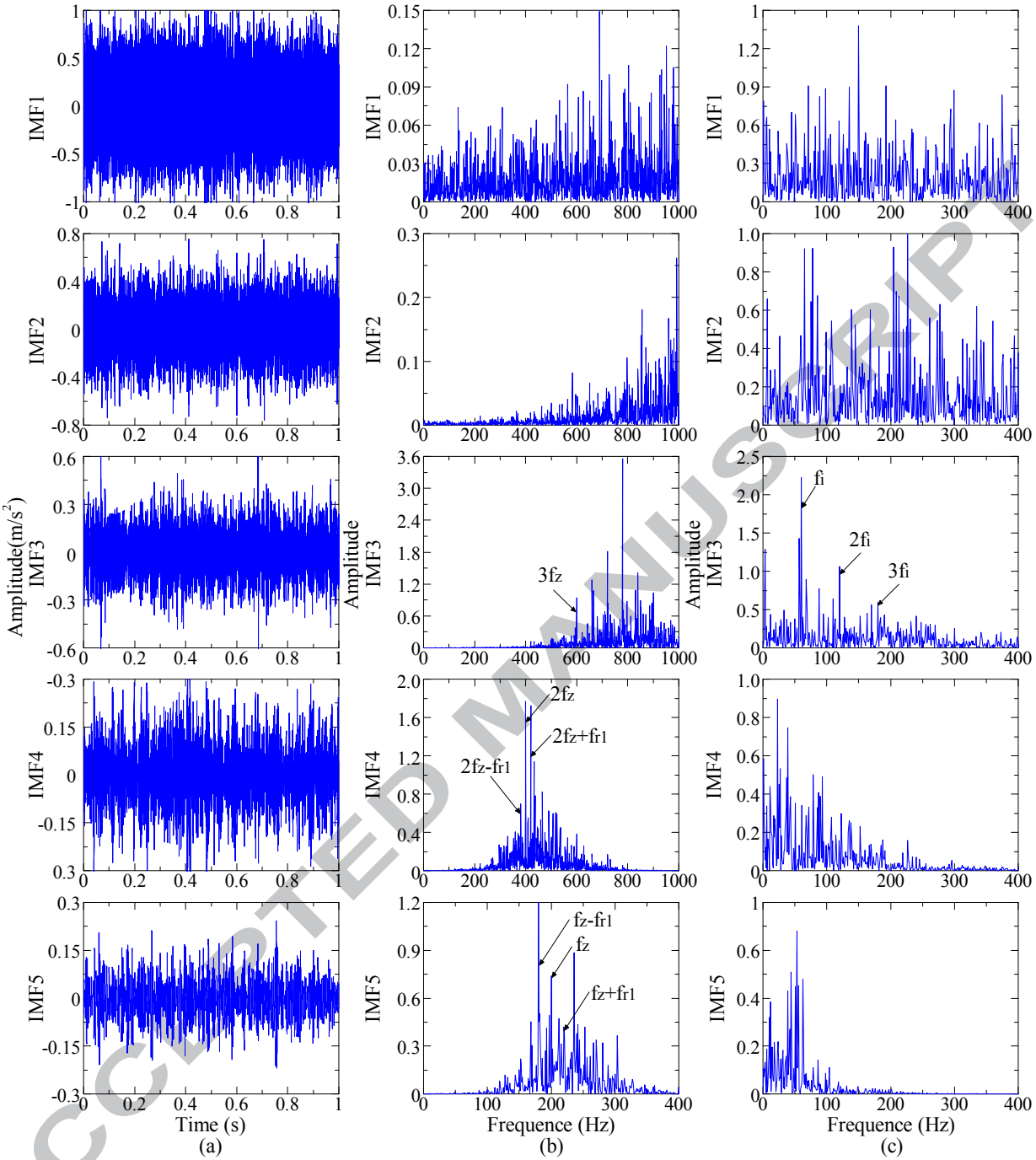

Fig. 6 Results of the mixed signal using EEMD: (a) time-domain graphs of first 5 IMFs; (b) power spectrum of (a); (c) envelope spectrum of (a).

Direct spectrum analysis cannot extract the fault features effectively. Although EEMD can extract the fault features of gear and bearing, the obtained power spectrum and envelope spectrum have too many interference spectral lines, which are prone to interfere the judgment of fault features. QGA-MCKD can effectively extract fault features, make the fault features clear and obvious, and make the fault type easy to identify. Therefore, the comparison of the processing results of the three methods proves the superiority of QGA-MCKD in compound fault feature recognition.

4.2. Application of QGA-MCKD in the experimental signal

The experimental signal of planetary gearbox, which comprised both planetary gear and bearing defects, was processed by QGA-MCKD to verify the practicality of the proposed method. The experiment was performed on a WTDS test platform, as shown in Fig. 7. WTDS is a comprehensive test platform for fault diagnosis of gearbox transmission, which contains replacement parts of fault gears and bearings. The test platform consists of two-stage fixed axis gear train and a planetary gear train, and the planetary gear train consists of three planetary gears. A variable frequency AC motor is used to drive the test platform with a rotating speed of 2400 r/min. Similar to the type of faults simulated by the simulated signal in section 4.1, the replacement parts of one planetary gear tooth breakage and bearing rolling element damage are used as shown in Fig. 8(a) and (b). A PCB accelerometer is attached on the outer shell of planetary gear train in the radial direction paralleling to the base to measure the vibration signal. The sampling frequency is set to 3000 Hz, and the installation location of accelerometer is shown in Fig. 8(c). The characteristic frequencies of multi-stage gear transmission system are shown in Table 2.

Table 2 Characteristic frequency of multi-stage gear transmission system of planetary gear

Fault characteristic frequency	frequency(Hz)
The meshing frequency of the first stage of fixed axis gear(f_1)	1159
The meshing frequency of the second stage of fixed axis gear(f_2)	417.1
The meshing frequency of the planetary gear(f_3)	101.6
The rotation frequency of AC motor (f_d)	40
The rotation frequency of the planetary gear (f_z)	2.819
The fault frequency of bearing rolling element damage(f_r)	6.3407

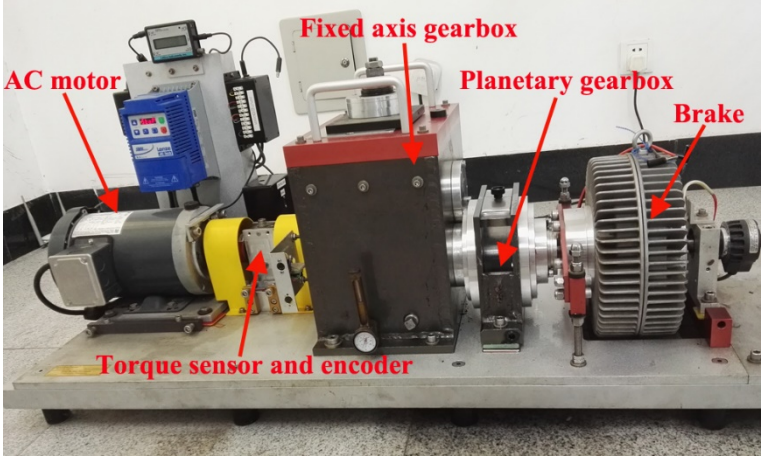

Fig. 7 WTDS test platform

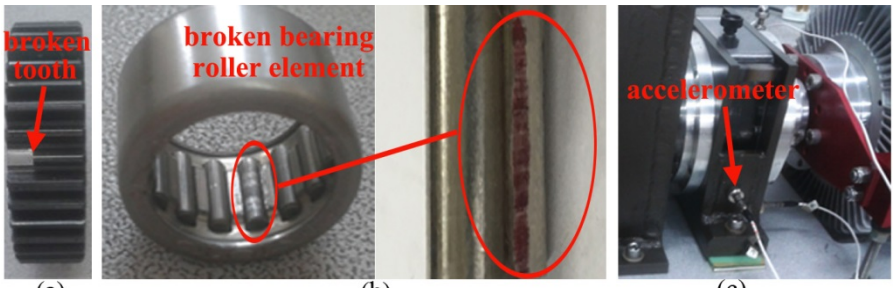

Fig. 8 (a) gear with one tooth breakage; (b) bearing with rolling element damage; (c) installation location of accelerometer

The acceleration signal was obtained after the test platform operating stably. The number of sampling points is 8192 and the time-domain graph is shown in Fig. 9(a). Fig. 9(b) is the power spectrum of the experimental signal, and Fig. 9(c) and 9(d) are partial enlarged views of Fig. 9(b) at 0-110 Hz and 90-320 Hz, respectively. As shown in Fig. 9, the meshing frequency of three velocity stages (f_1, f_2 and f_3) can be seen, but the characteristic frequencies are difficult to distinguish because of noise interference. Especially the amplitude of planetary gear meshing frequency (f_3) is the smallest. The second and third harmonics of f_3 also can be seen in Fig. 9(d), but they are hard to identify because the amplitude of which are very small. The envelope spectrum of experimental signal is shown in Fig. 9(e), where fault frequency of bearing (f_r) cannot be seen. Direct spectrum analysis cannot identify compound fault features from vibrational signals contaminated by noise.

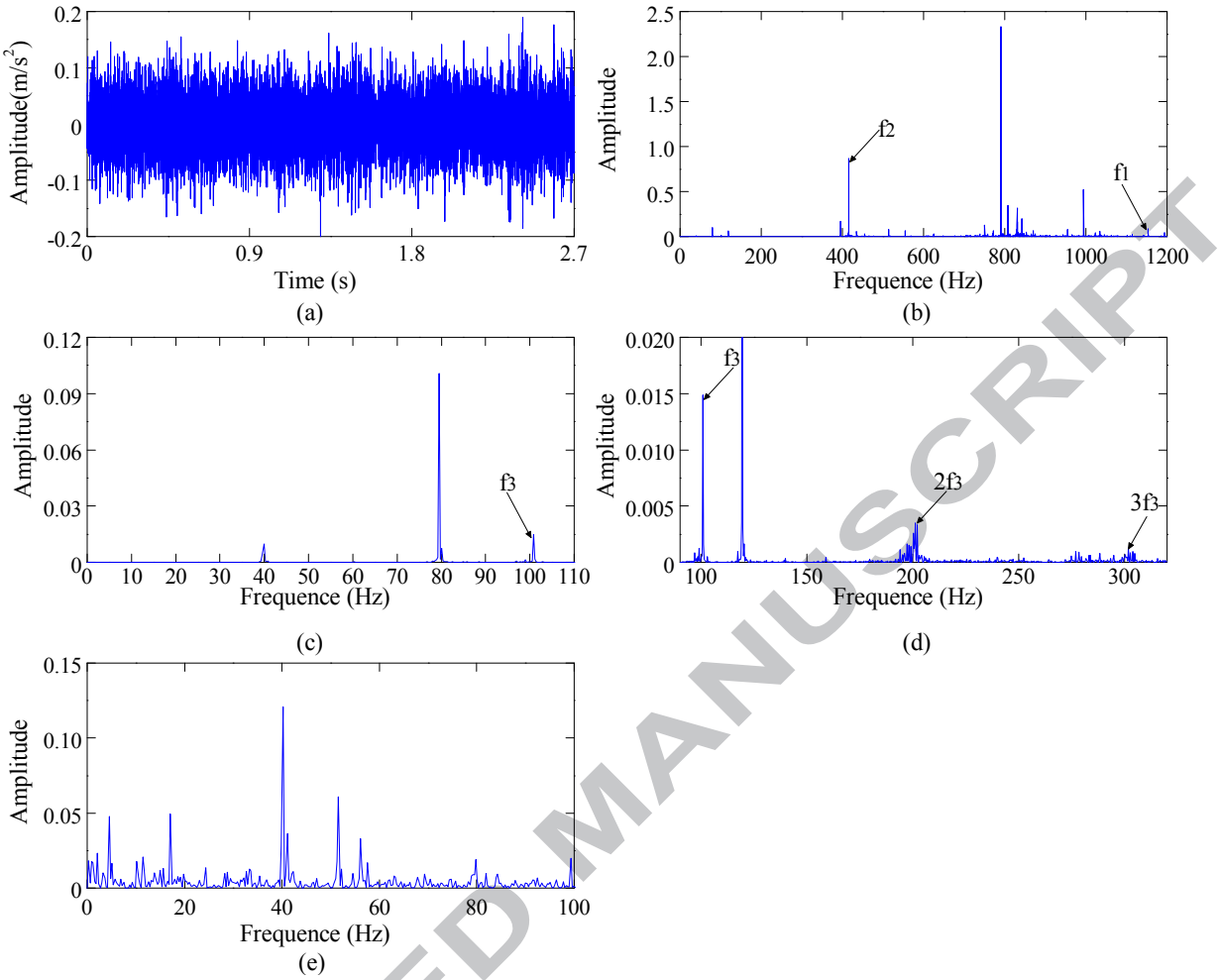

Fig. 9 Time-domain graph and frequency spectrum of the experimental signal: (a) time-domain graph of the experimental signal; (b) power spectrum of the experimental signal; (c) partial enlargement of (b) at 0-110Hz; (d) partial enlargement of (b) at 90-320Hz; (e) envelop spectrum of the experimental signal.

Ensure T is within the range of approximately 20–300 when using MCKD. If T is in excess of this range, the dataset should firstly be resampled [21]. In order to make T within a reasonable range, the raw signal needs to be resampled. The resampling frequency of the gear fault signal is set to 12000 Hz, and that of the fault bearing signal is set to 1500 Hz. According to equation (3), the T of gear and bearing are 118 and 237, and the optimization range of T is set to (98, 138) and (217, 257), respectively.

In order to verify the advantages of QGA in MCKD parameter selection, comparison was performed among QGA, GA and CSA. The EE value of the experimental signal obtained by the optimization algorithms and the iteration number needed to find the optimal solution were used as the comparison basis.

The variables of the three optimization algorithm were initialized as follows: the population size was set to 30, the maximum number of iterations was set to 200, the selection range of L was set to

(2,700), and the parameter T of gear and bearing were set to (98,138) and (217,257), respectively. The comparison of convergence curves are shown in Fig. 10.

It can be seen from Fig. 10(a) that in the gear parameter optimization, QGA finds the optimal result in the 35th generation, and the EE value obtained by QGA is the smallest; GA finds the optimal result in the 62nd generation, which is the largest; and the EE value obtained by CSA is the largest. Therefore, the optimal solution of QGA in the calculation of gear signal is the best among the three algorithms.

As shown in Fig. 10(b), when searching for the optimal parameters of the bearing, QGA finds the optimal solution in the 37th generation, and the EE value obtained by QGA is the smallest; the iteration number for the optimal solution by GA is the largest, and the EE value found by GA is also the largest; CSA finds the optimal solution in the 25th generation, which is the smallest of all, but the EE value obtained by CSA is larger than QGA. Although the iteration number of CSA using to find the optimal solution is smaller than that of QGA, the difference between the two is not large, so it is considered that the optimal solution of QGA for the bearing signal is the best among the three algorithms.

QGA and CSA run independently for 15 times, and the iteration number is 200, obtaining convergence curves of the average of EE value as shown in Fig. 11. It can be seen from Fig. 11(a) that the optimal solution of QGA for gear parameter optimization is better than that of CSA; in the bearing parameters optimization, the trend of the curves are the same as that in Fig. 10(b). When the iteration number is small, the optimal solution obtained by CSA is better than that of QGA, but with the increasing of iteration number, the final optimal solution of QGA is better than CSA. The variance of optimal solution obtained by QGA is 4.756×10^{-4} and that of CSA is 5.396×10^{-4}. The comparisons show that the stability in parameter optimization of QGA is better than that of CSA.

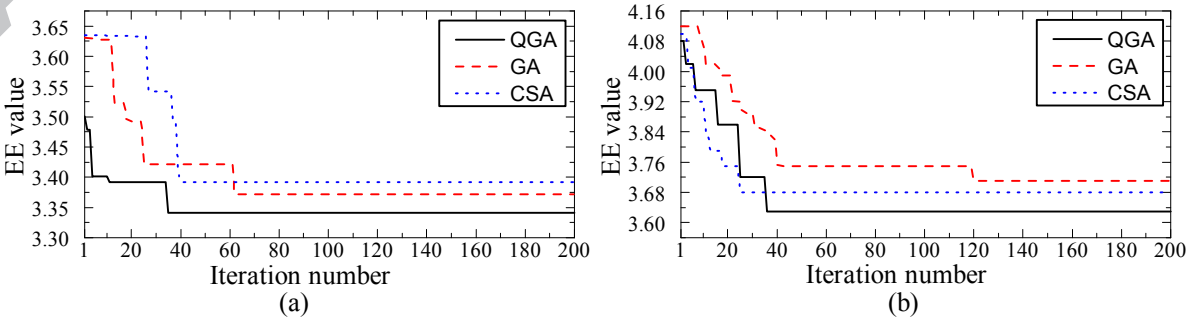

Fig. 10 The comparison results of QGA, GA and CSA: (a) the optimal solution comparison of the gear signal; (b) the optimal solution comparison of the bearing signal.

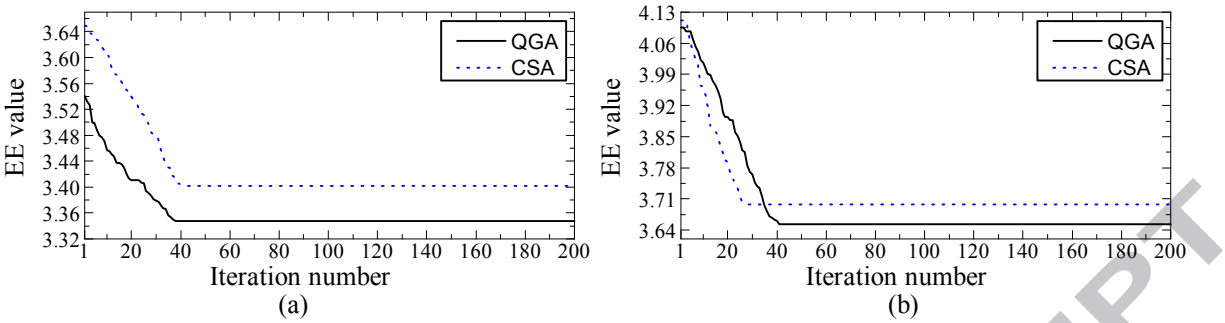

Fig. 11 Convergence curves comparison of the average of EE value between QGA and CSA: (a) the optimal solution comparison of the gear signal; (b) the optimal solution comparison of the bearing signal.

QGA was used to optimize the MCKD parameter combinations of gear and bearing fault features. And the optimization results are shown in Figure 12(a) and (b).

As show in Fig. 12(a) and (b), with the increasing of iteration number, the EE value of the fault signal obtained by QGA decreases continuously. When the iteration number reaches the 35th generation, the optimal solution of the parameter combination of gear fault signal is stable, and the EE value obtained is 3.34. When the iteration number reaches the 37th generation, the optimal solution of the parameter combination of bearing fault signal is stable, and the EE value obtained is 3.62. The optimal parameter combination of the gear fault signal is L=500, T=119 and that of the bearing fault signal is L=21, T=237.

The optimal parameters were assigned to MCKD to process the experimental signal, and the gear and bearing fault signals were obtained, respectively, as shown in Fig. 12(c) and (d). The power spectrum of gear fault signal is shown in Fig. 12(e) and (g), from which the meshing frequency of planetary gear and its harmonics are the main components, and the side frequency components generated by the gear rotation frequency modulation also can be seen. Compared with Fig. 9(b) (c) (d), QGA-MCKD has a better noise filtering effect, and completely highlights the main frequency components of the fault gear. Compared with Fig. 9(e), Fig. 12(f) shows that the fault frequency and the harmonic components of the fault bearing are very obvious, and the high-order harmonic components are also can be seen. These results indicate that QGA-MCKD can effectively extract compound fault components lost in background noise.

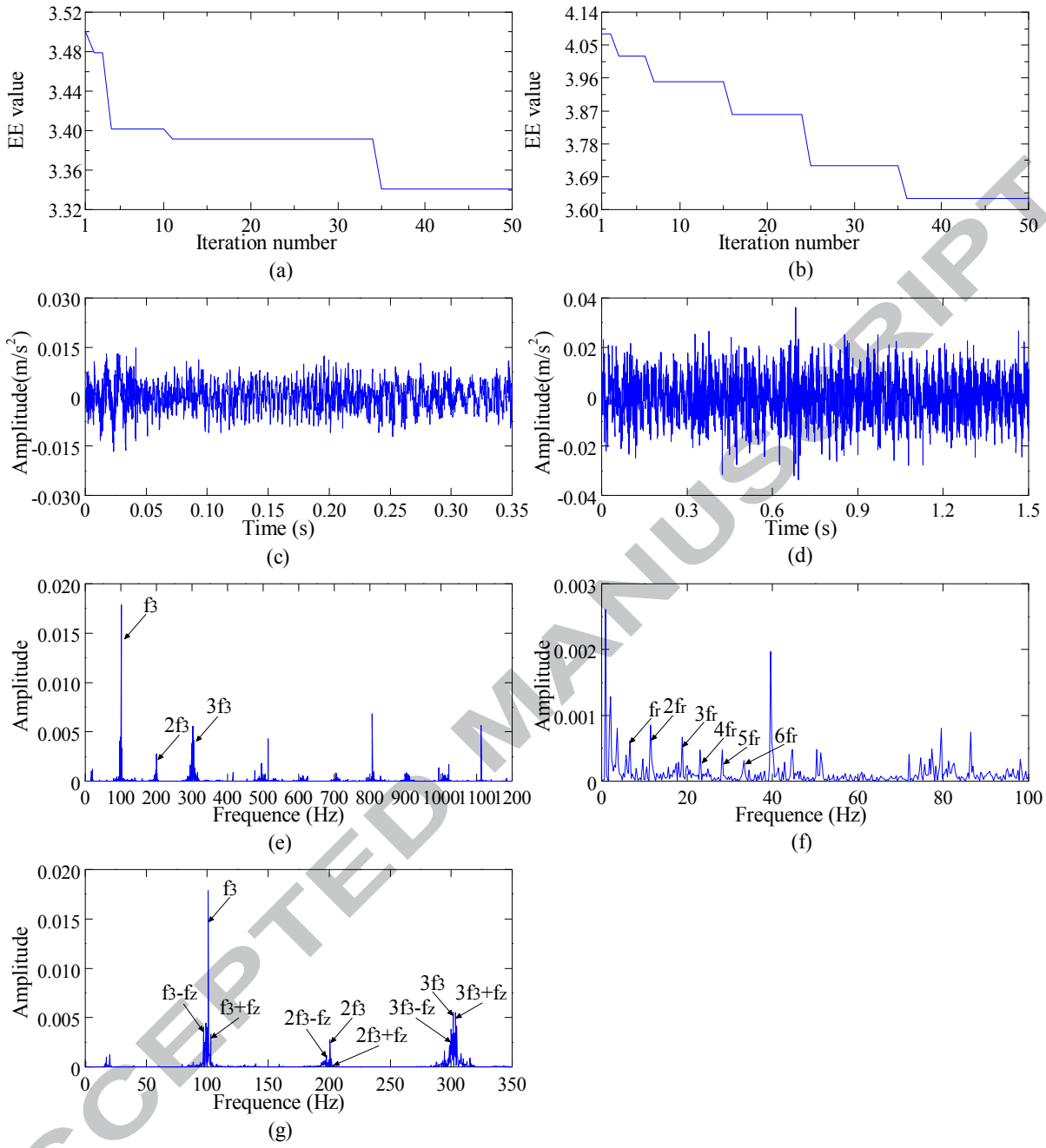

Fig. 12 Results of the experimental signal using QGA-MCKD: (a) and (b) convergence curves of QGA for extracting the gear and bearing fault signals, respectively; (c) and (d) time-domain graphs of the extracted gear and bearing fault signals, respectively; (e) power spectrum of (c); (f) envelope spectrum of (d); (g) partial enlargement of (e) at 0-350Hz.

It can be seen from the comparison between QGA-MCKD and direct spectrum analysis that the proposed method can extract fault feature components from the mixed signal contaminated by noise. In order to further verify the superiority of the proposed method, a mature fault diagnosis method EEMD was adopted to compare with QGA-MCKD. The same experimental signals were processed by the two methods, respectively, and the results were compared and verified.

The experimental signal was processed by EEMD, and 12 IMFs were acquired, of which the first 4 IMFs contained useful information. The power spectrum is shown in Fig. 13(b), where f_1, f_2

and f_3 can be seen. However, in the 0-400Hz band, only the meshing frequency of planetary gear can be found, and the characteristic frequency related to planetary gear tooth breakage such as harmonics of meshing frequency and the side frequency generated by gear rotation frequency modulation are disturbed by irrelevant spectral lines. The envelope spectrum shown in Fig. 13(c) can extract the bearing fault frequency and its harmonics, but the frequency components are difficult to identify because of many interference spectral lines, which makes it difficult to identify the fault type.

Compared with Fig. 13(b), it can be seen in Fig. 12(g) that the noise filtering effect using QGA-MCKD is much better, and the main frequency components of fault gear are completely extracted. In the envelope spectrum of the bearing fault signal shown in Fig. 12(f), the bearing fault frequency (f_r) and its harmonic components are obvious, and high order harmonics also can be seen. Compared with the envelope spectrum obtained by EEMD in Fig. 13(c), Fig. 12(f) shows that the main frequency components are clearer, the high order harmonic components of f_r are more prominent, and the fault feature of the bearing can be recognized more easily. These results demonstrate the effectiveness of the proposed method.

EEMD can decompose signal into different frequency bands, but the decomposed IMF has the problem that the characteristic frequency is disturbed by the unrelated spectral lines. QGA-MCKD can develop the advantages of MCKD in signal processing and highlight the periodic components of interest. Compared with EEMD, the period components of signals processed by QGA-MCKD are more obvious, the fault frequency can be recognized more easily and the fault characteristics of planetary gearbox compound faults can be extracted more effectively.

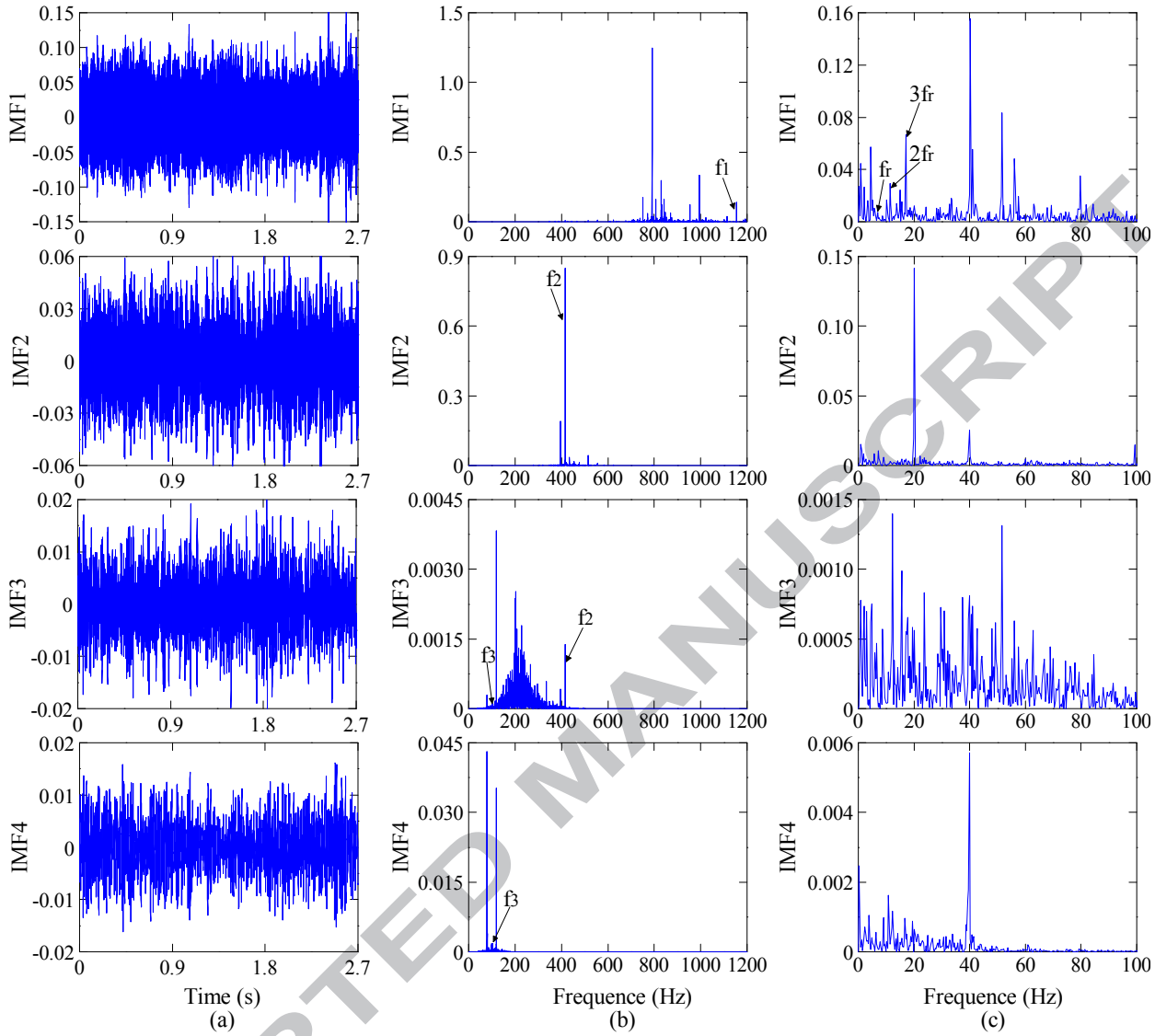

Fig. 13 Results of the experimental signal using EEMD: (a) time-domain graphs of first 4 IMFs; (b) power spectrum of (a); (c) envelope spectra of (a).

In order to verify the stability and practicability of the proposed method, QGA-MCKD was applied to diagnose the compound fault of planetary gear tooth wear and bearing outer race fault. In the power spectrum of the gear fault signal extracted by QGA-MCKD, the meshing frequency of planetary gear and its 2nd and 3rd harmonics were the main frequency components. The 4th harmonic was weak but identifiable, and the amplitude of the harmonics of meshing frequency were significantly larger than that of normal state. The frequency characteristics clearly indicated the fault of gear tooth wear. In the envelope spectrum of the bearing fault signal extracted by QGA-MCKD, the fault frequency of bearing outer race and its high order harmonics were the main frequency components. The fault characteristics of bearing outer race could be identified clearly.

Compared with the existing methods [25, 32], QGA has advantages in the selection of key

parameters of MCKD. The existing methods were only used for bearing compound fault diagnosis, but the proposed method was successfully applied to diagnose gear and bearing compound faults. QGA-MCKD has been successfully applied to the compound fault diagnosis of gear tooth breakage and bearing rolling element damage, and gear tooth wear and bearing outer race fault, which proves its practicability and stability, and expands the application range of adaptive MCKD method in compound fault diagnosis.

5. Conclusion

This paper proposed an improved MCKD method based on QGA (QGA-MCKD) for gear and bearing compound fault diagnosis. The performance of MCKD was improved by employing QGA to adaptively select the key parameters (T and L) of MCKD. The proposed method was successfully applied to the diagnosis of compound fault of planetary gearbox.

Compared with GA and CSA, QGA gained the best optimal solution and showed the best stability in MCKD parameter optimization. QAG-MCKD was applied to the compound fault diagnosis of one planetary gear tooth breakage and bearing rolling element damage. In the power spectrum of the extracted gear fault signal, the main frequency components which could reflect the fault of planetary gear tooth breakage were highlighted. In the envelop spectrum of the extracted bearing fault signal, the frequency of bearing roller element damage and its harmonics components were obvious. Compared with the direct spectrum analysis and EEMD, QGA-MCKD could extract single fault signals from the compound fault signal more effectively. The proposed method was applied to the compound fault diagnosis of gear tooth wear and bearing outer race fault. The fault features of two single faults were successfully extracted to realize the compound fault diagnosis, which verified the stability of the method.

The simulated and experimental results indicate that the adaptive selection of parameters using QGA can improve the performance of MCKD. QGA-MCKD has strong advantages in weak fault diagnosis, which is an effective compound fault diagnosis method to extract single fault signal from complex signal in planetary gearbox.

Reference

[1] H. Pan, Y. Yang, X. Li, J. Zheng, J. Cheng, Symplectic geometry mode decomposition and its application to rotating machinery compound fault diagnosis, Mechanical Systems & Signal Processing, 114 (2019) 189-211.

[2] S. He, J. Chen, Z. Zhou, Y. Zi, Y. Wang, X. Wang, Multifractal entropy based adaptive multiwavelet construction and its application for mechanical compound-fault diagnosis, Mechanical Systems & Signal Processing, s 76–77 (2016) 742-758.

[3] T. Wang, F. Chu, Q. Han, Y. Kong, Compound faults detection in gearbox via meshing resonance and spectral kurtosis methods, Journal of Sound and Vibration, 392 (2017) 367-381.

[4] H. Taplak, S. Erkaya, İ. Uzmay, Experimental analysis on fault detection for a direct coupled rotor-bearing system, Measurement, 46 (2013) 336-344.

[5] A. Glowacz, W. Glowacz, Vibration-Based Fault Diagnosis of Commutator Motor, Shock and Vibration, 2018 (2018) 1-10.

[6] S. Lu, Q. He, J. Zhao, Bearing fault diagnosis of a permanent magnet synchronous motor via a fast and online order analysis method in an embedded system, Mechanical Systems and Signal Processing, 113 (2018) 36-49.

[7] C. Delpha, D. Diallo, H. Al Samrout, N. Moubayed, Multiple incipient fault diagnosis in three-phase electrical systems using multivariate statistical signal processing, Engineering Applications of Artificial Intelligence, 73 (2018) 68-79.

[8] X. Chen, Z. Feng, Time-frequency space vector modulus analysis of motor current for planetary gearbox fault diagnosis under variable speed conditions, Mechanical Systems and Signal Processing, 121 (2019) 636-654.

[9] F. Cheng, Y. Peng, L. Qu, W. Qiao, Current-Based Fault Detection and Identification for Wind Turbine Drivetrain Gearboxes, 2016.

[10] A. Glowacz, Fault diagnosis of single-phase induction motor based on acoustic signals, Mechanical Systems and Signal Processing, 117 (2019) 65-80.

[11] A. Glowacz, Acoustic-Based Fault Diagnosis of Commutator Motor, Electronics, 7 (2018) 299.

[12] A. Parey, A. Singh, Gearbox fault diagnosis using acoustic signals, continuous wavelet transform and adaptive neuro-fuzzy inference system, Applied Acoustics, (2018).

[13] V.T. Tran, B.S. Yang, F. Gu, A. Ball, Thermal image enhancement using bi-dimensional empirical mode decomposition in combination with relevance vector machine for rotating machinery fault diagnosis, Mechanical Systems & Signal Processing, 38 (2013) 601-614.

[14] O. Janssens, R. Schulz, V. Slavkovikj, K. Stockman, M. Loccufier, R.V.D. Walle, S.V.

Hoecke, Thermal image based fault diagnosis for rotating machinery, Infrared Physics & Technology, 73 (2015) 78-87.

[15] A. Glowacz, Z. Glowacz, Diagnosis of the three-phase induction motor using thermal imaging, Infrared Physics & Technology, 81 (2016) 7-16.

[16] Z.P. Feng, L.L. Zhao, F.L. Chu, Vibration Spectral Characteristics of Localized Gear Fault of Planetary Gearboxes, Proceedings of the Chinese Society for Electrical Engineering, 33 (2013) 118-125.(Chinese)

[17] AIAA, Detection and Localization of Tooth Breakage Fault on Wind Turbine Planetary Gear System considering Gear Manufacturing Errors, Shock and Vibration, 2014,(2014-8-19), 2014 (2014) 1-13.

[18] X.H. Chen, G. Cheng, X.L. Shan, X. Hu, Q. Guo, H.G. Liu, Research of weak fault feature information extraction of planetary gear based on ensemble empirical mode decomposition and adaptive stochastic resonance, Measurement, 73 (2015) 55-67.

[19] Y. Li, G. Cheng, Y. Pang, M. Kuai, Planetary Gear Fault Diagnosis via Feature Image Extraction Based on Multi Central Frequencies and Vibration Signal Frequency Spectrum, Sensors, 18 (2018) 1735.

[20] M. He, D. He, J. Yoon, T.J. Nostrand, J. Zhu, E. Bechhoefer, Wind turbine planetary gearbox feature extraction and fault diagnosis using a deep-learning-based approach, Proceedings of the Institution of Mechanical Engineers, Part O: Journal of Risk and Reliability, 0 1748006X18768701.

[21] L.S. Dhamande, M.B. Chaudhari, Compound gear-bearing fault feature extraction using statistical features based on time-frequency method, Measurement, 125 (2018) 63-77.

[22] G. Cai, X. Chen, Z. He, Sparsity-enabled signal decomposition using tunable Q-factor wavelet transform for fault feature extraction of gearbox, Mechanical Systems and Signal Processing, 41 (2013) 34-53.

[23] D. Yu, M. Wang, X. Cheng, A method for the compound fault diagnosis of gearboxes based on morphological component analysis, Measurement, 91 (2016) 519-531.

[24] H. Jiang, C. Li, H. Li, An improved EEMD with multiwavelet packet for rotating machinery multi-fault diagnosis, Mechanical Systems & Signal Processing, 36 (2013) 225-239.

[25] G. Tang, X. Wang, Y. He, Diagnosis of compound faults of rolling bearings through adaptive

maximum correlated kurtosis deconvolution, Journal of Mechanical Science & Technology, 30 (2016) 43-54.

[26] D. Zhang, D. Yu, Multi-fault diagnosis of gearbox based on resonance-based signal sparse decomposition and comb filter, Measurement, 103 (2017) 361-369.

[27] Z. Li, X. Yan, Z. Tian, C. Yuan, Z. Peng, L. Li, Blind vibration component separation and nonlinear feature extraction applied to the nonstationary vibration signals for the gearbox multi-fault diagnosis, Measurement Journal of the International Measurement Confederation, 46 (2013) 259-271.

[28] Y. Song, S. Zeng, J. Ma, J. Guo, A fault diagnosis method for roller bearing based on empirical wavelet transform decomposition with adaptive empirical mode segmentation, Measurement, 117 (2018) 266-276.

[29] B. Li, P.-l. Zhang, H. Tian, S.-s. Mi, D.-s. Liu, G.-q. Ren, A new feature extraction and selection scheme for hybrid fault diagnosis of gearbox, Expert Systems with Applications, 38 (2011) 10000-10009.

[30] J. Feng, Y. Lei, H. Shan, L. Jing, Early Fault Diagnosis of Bearings Using an Improved Spectral Kurtosis by Maximum Correlated Kurtosis Deconvolution, Sensors, 15 (2015) 29363.

[31] H. Lianhuan, L. Xiaobo, Z. Hongyan, Compound fault diagnosis of rotating machinery based on adaptive maximum correlated kurtosis deconvolution and customized multiwavelet transform, Measurement Science and Technology, 29 (2018) 115007.

[32] Y. Miao, M. Zhao, J. Lin, Y. Lei, Application of an improved maximum correlated kurtosis deconvolution method for fault diagnosis of rolling element bearings, Mechanical Systems & Signal Processing, 92 (2017) 173-195.

[33] G. L. McDonald, Q. Zhao, M. J. Zuo, Maximum correlated Kurtosis deconvolution and application on gear tooth chip fault detection, Mechanical Systems & Signal Processing, 33 (2012) 237-255.

[34] K.H. Han, K.H. Park, C.H. Lee, J.H. Kim, Parallel quantum-inspired genetic algorithm for combinatorial optimization problem, Evolutionary Computation, 2001. Proceedings of the 2001 Congress on, 2001, pp. 1422-1429 vol. 1422.

[35] B. Li, Z.Q. Zhuang, Genetic Algorithm Based-On the Quantum Probability Representation,

Lecture Notes in Computer Science, 2412 (2002) 500-505.

[36] G. Zhang, W. Jin, N. Li, An Improved Quantum Genetic Algorithm and Its Application, Rough Sets, Fuzzy Sets, Data Mining, and Granular Computing, International Conference, Rsfdgrc 2003, Chongqing, China, May 26-29, 2003, Proceedings, 2003, pp. 449-452.

[37] K.H. Han, J.H. Kim, Genetic quantum algorithm and its application to combinatorial optimization problem, Evolutionary Computation, 2000. Proceedings of the 2000 Congress on, 2002, pp. 1354-1360 vol.1352.

[38] Z. Wu, N. Huang, X. Chen, The Multi-Dimensional Ensemble Empirical Mode Decomposition Method, 2009.

[39] Y. Zhang, C. Zhang, J. Sun, J. Guo, Improved Wind Speed Prediction Using Empirical Mode Decomposition, 2018.

1. A novel gearbox compound fault diagnosis method is proposed.
2. The method relies on improved maximum correlated kurtosis deconvolution method based on quantum genetic algorithm.
3. The method is successfully applied to diagnose compound fault of planetary gear and bearing.
4. The method expands the application range of adaptive MCKD method in compound fault diagnosis of gearbox.